Advanced Droop Control in Islanded Microgrids Using Dynamic Phasor Models

Christoph Kammer and Alireza Karimi

Automatic Control Laboratory
(e-mail: christoph.kammer@epfl.ch, alireza.karimi@epfl.ch)
Ecole Polytechnique Fédérale de Lausanne (EPFL), Switzerland

Abstract: A dynamic phasor model for low- and medium-voltage distribution grids is presented. This model accurately represents the transient dynamics of this type of grid, and its low order makes it well suited for control design. A novel fixed-structure, robust control design method based on convex optimization is then used to design a decentralized low-order controller that shows a significantly improved transient performance compared to classical droop controllers. The performance of the designed controller is then validated in a simulation example for voltage and frequency control of an islanded medium-voltage distribution grid.

Keywords: Power-System Control, Robust Control, Convex Optimization

1. INTRODUCTION

The steady increase of renewable and distributed energy resources in electric power grids is presenting a significant challenge for the stability and reliability of the future electrical network. The classical layout of the electrical grid, with few centralized generation units connected at the high-voltage level, is replaced by a new structure, where many small distributed generation (DG) units are connected at the mid- or low-voltage level. Distributed sources are often connected through voltage source inverters (VSIs). Parallel operation and control of VSIs has been an active topic in the literature in recent times especially for islanded grids. The issues of transient frequency and voltage stability are much more pronounced in this type of grids, and systematic controller design for parallel VSIs is still an open research question.

Key features of droop control are its decentralized architecture, and the guarantee of proportional power sharing between DG units. However, droop control also has several drawbacks. It is unable to compensate coupling effects between parallel inverters, can not account for the dynamics of the DG units and exhibits poor performance in grids with mixed lines. Adaptations of the classical droop control method to parallel VSIs have been extensively studied in the literature (see Bidram and Davoudi (2012); Guerrero et al. (2011)). In Guerrero et al. (2007); Zhong (2013), digital filters are designed to reduce harmonic oscillations between droop-controlled inverters. However, no model is used during the design process, and closed-loop stability and performance are only evaluated in retrospect.

From a control design perspective, droop control is a model-free design approach, where the droop gains are tuned experimentally. A major issue that will be addressed in this work is the lack of a suitable model for classical control design. For classical analysis, power grids are commonly modeled as small signal models. However, this model becomes prohibitively complex even for medium-sized grids and requires detailed knowledge of the DG units' characteristics. Another approach is to use reduced-order small signal models, but this neglects the transient dynamics, so the results are not accurate for fast, inverter-based grids. The closed-loop stability of droop control under some assumptions has been proven in Simpson-Porco et al. (2013); Schiffer et al. (2014). However, these works use a nonlinear quasi-static formulation of the power flows, which leads to the inaccurate conclusion that the system is stable for arbitrary droop gains.

Therefore, in the first part of this paper a dynamic model of an inverter-based microgrid using a dynamic phasor approach will be presented. This model is able to accurately represent the electromagnetic and electromechanical dynamics of a low- or medium-voltage distribution grid, while having a significantly reduced complexity compared to a small-signal model. While this type of model has been used for stability analysis in Nazari and Ilic (2014); Guo et al. (2014), and for control design of single inverters in Brabandere (2006), its application to control design with multiple parallel inverters has not been explored so far. In the second part of this paper, a novel method to design fixed-structure robust controllers based on the frequency response of multivariable systems and convex optimization is presented. The dynamic phasor model will then be used to design a decentralized low-order controller that shows a significantly improved transient performance compared to droop control. The performance of the new controller is validated in a simulation example of a real medium-voltage grid with mixed lines.

2. DYNAMIC PHASOR MODEL

In this section, a novel model for low- and medium-voltage grids is presented. As mentioned in the previous section, the conventionally used models are not well suited for

⋆ The work presented in this paper was supported by the Swiss Federal Commission for Innovation and Technology within the SCCER-FURIES.

controller synthesis in grids with a large amount of VSIs, where electromagnetic dynamics play a significant role. To resolve this issue, a frequency-domain model based on a dynamic phasor approach is developed that is able to accurately describe the dynamics of the grid frequency, bus voltages and power flows, while having a significantly reduced complexity compared to a small-signal model. The model is able to incorporate the dynamics of any number of DG units as well as constant power loads, resulting in a simple formulation that is well suited for control design.

2.1 Dynamic Power Flow Equations

The balanced, three-phase voltage at bus i can be represented in the phasor notation:

$$U_i \angle \theta_i = \sqrt{2} U_i(t) \begin{bmatrix} cos(\bar{\omega}t + \theta_i(t)) \\ cos(\bar{\omega}t + \theta_i(t) - 2\pi/3) \\ cos(\bar{\omega}t + \theta_i(t) + 2\pi/3) \end{bmatrix} \quad (1)$$

with θ_i, U_i being the voltage angle in rad and the line-to-ground RMS magnitude at bus i, and $\bar{\omega}$ being the nominal grid frequency in rad/s. The argument (t) will generally be omitted for simplicity.

For low- and medium-voltage distribution grids, lines can be modeled as R-L elements. The transfer functions of the linearized dynamic power flow equations in such a line are as follows (see Venkatasubramanian et al. (1995)):

$$\begin{aligned} P_{ij} = {} & 3 \frac{\bar{\omega} L_{ij}}{(L_{ij}s + R_{ij})^2 + (\bar{\omega} L_{ij})^2} \bar{U}^2 \frac{1}{s} (\omega_i - \omega_j) \\ & + 3 \frac{L_{ij}s + R_{ij}}{(L_{ij}s + R_{ij})^2 + (\bar{\omega} L_{ij})^2} \bar{U} (U_i - U_j) \quad (2) \\ Q_{ij} = {} & 3 \frac{\bar{\omega} L_{ij}}{(L_{ij}s + R_{ij})^2 + (\bar{\omega} L_{ij})^2} \bar{U} (U_i - U_j) \\ & + 3 \frac{L_{ij}s + R_{ij}}{(L_{ij}s + R_{ij})^2 + (\bar{\omega} L_{ij})^2} \bar{U}^2 \frac{1}{s} (\omega_i - \omega_j) \quad (3) \end{aligned}$$

where P_{ij}, Q_{ij} are active and reactive power transmitted from bus i to bus j, R_{ij}, L_{ij} are resistance and inductance of the line, ω_i is the grid frequency in rad/s at bus i and $\bar{U}$ is the nominal line-to-ground RMS voltage.

2.2 Grid Transfer Function

We assume that every bus in the grid is connected to either a DG unit or a load, and that any zero-injection buses have been eliminated (e.g. using Kron reduction). Then, dividing the buses into VSI buses and load buses, we can write:

$$\begin{bmatrix} P_{\mathcal{I}} \\ Q_{\mathcal{I}} \\ P_{\mathcal{L}} \\ Q_{\mathcal{L}} \end{bmatrix} = \begin{bmatrix} G_1 & G_2 \\ G_3 & G_4 \end{bmatrix} \begin{bmatrix} \omega_{\mathcal{I}} \\ U_{\mathcal{I}} \\ \omega_{\mathcal{L}} \\ U_{\mathcal{L}} \end{bmatrix} \quad (4)$$

Let g be the number of VSI buses and let l be the number of load buses in the grid. $P_{\mathcal{I}}, Q_{\mathcal{I}} \in \mathbf{R}^{g \times 1}$ are vectors with the active and reactive output power of the VSIs, and $P_{\mathcal{L}}, Q_{\mathcal{L}} \in \mathbf{R}^{l \times 1}$ are vectors with the active and reactive power of the loads. Load power (i.e. power going out of the grid) has a negative sign. $\omega_{\mathcal{I}}, U_{\mathcal{I}} \in \mathbf{R}^{g \times 1}$ are vectors with the grid frequency and voltage magnitude at the generator buses, $\omega_{\mathcal{L}}, U_{\mathcal{L}} \in \mathbf{R}^{l \times 1}$ are vectors with the grid frequency and voltage magnitude at the load buses. The matrix transfer functions $G_i (i = 1, 2, 3, 4)$ are constructed using the power flow transfer functions presented in Section 2.1, where G_1 is of dimension $2g \times 2g$, G_2 of $2g \times 2l$, G_3 of $2l \times 2g$ and G_4 of $2l \times 2l$.

Assuming constant power loads, the dynamics are reformulated such that the power drawn by the loads enters the system as a disturbance. Thus, the power flow of the generator buses can be written as a function of the generator bus phasors, with the load power acting as a disturbance:

$$\begin{bmatrix} P_{\mathcal{I}} \\ Q_{\mathcal{I}} \end{bmatrix} = G_{\text{grid}} \begin{bmatrix} \omega_{\mathcal{I}} \\ U_{\mathcal{I}} \end{bmatrix} + G_d \begin{bmatrix} P_{\mathcal{L}} \\ Q_{\mathcal{L}} \end{bmatrix} \quad (5)$$

with $G_{\text{grid}} = G_1 - G_2 G_4^{-1} G_3, \quad G_d = G_2 G_4^{-1}$.

Remark: The dynamic phasor model is able to incorporate both VSI-interfaced sources as well as synchronous machines. Further, grey- and black-box models of DG units can directly be included. An expanded version of the model can be found in Kammer and Karimi (2017).

2.3 Dynamic Phasor Model

To demonstrate the exactness of the modeling approach, a dynamic phasor model of an example grid is created. To validate the results, the same grid is implemented in Simulink using the Simpower toolbox, and the response of the systems to a load change is compared.

A grid model based on the three-phase islanded Subnetwork 1 of the CIGRE benchmark medium voltage distribution network is used Rudion et al. (2006). The network is a meshed network with mixed lines consisting of 11 buses (see Fig. 1). The following modifications are made compared to the original system: Only 3 VSI-interfaced battery storage units connected to buses 5, 9 and 10 are considered. The inverters are connected to the grid through an L-type output filter. The photovoltaics are assumed to operate in maximum power point tracking mode and are absorbed into the loads. The loads at buses 1, 5, 9 and 10 are neglected. Since the grid is running in islanded mode, the loads and power ratings of the DG units are scaled such that nominal generation and load is at an equilibrium. To prevent the dynamics from being dominated by a single VSI, the power ratings are in a similar range for all units.

The inverters are operating in Frequency-Voltage mode and modeled as ideal voltage sources with the following first-order dynamics:

$$\begin{bmatrix} \omega_{\mathcal{I}} \\ U_{\mathcal{I}} \end{bmatrix} = G_{DG} \begin{bmatrix} \bar{\omega}_{\mathcal{I}} \\ \bar{U}_{\mathcal{I}} \end{bmatrix}; \; G_{DG} = \frac{1}{2 \times 10^{-4} s + 1} I \quad (6)$$

where $\bar{\omega}_{\mathcal{I}}, \bar{U}_{\mathcal{I}}$ are the reference VSI frequency and voltage magnitude, and I is the identity matrix with dimension $2g \times 2g$. The inverters are controlled using droop control :

$$\bar{\omega}_{\mathcal{I}} = k_p (\bar{P}_{\mathcal{I}} - P_{\mathcal{I}}) \;\; ; \;\; \bar{U}_{\mathcal{I}} = k_q (\bar{Q}_{\mathcal{I}} - Q_{\mathcal{I}}) \quad (7)$$

where k_p, k_q are diagonal matrices containing the droop gains and $\bar{P}_{\mathcal{I}}, \bar{Q}_{\mathcal{I}}$ are the reference active and reactive power of the batteries, which are assumed to be given by a higher-level controller.

The line impedances of the grid are given in Rudion et al. (2006), the other grid parameters are listed in Table 1, where L_f, R_f denotes the impedance of the VSI output filters. The active power droop gains k_p are chosen such that proportional load sharing is maintained.

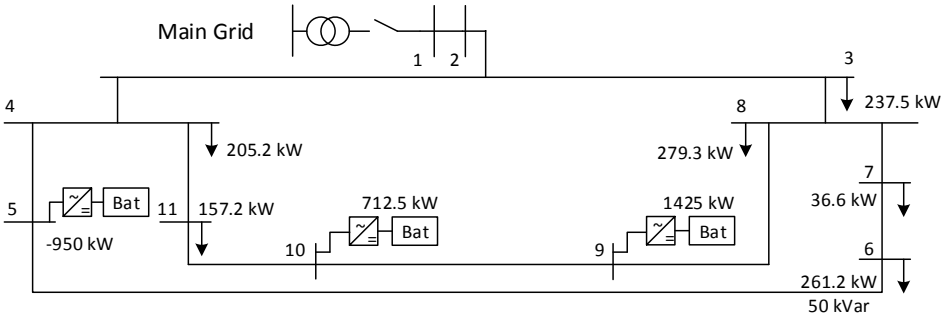

Fig. 1. Model adapted from Rudion et al. (2006) with 11 buses, 3 inverter-interfaced batteries and 6 loads. The sign ↓ denotes the loads.

Table 1. Test Grid Parameters

Base Values	S_{base} = 4.75 MVA, U_{base} = 20 kV, f = 50 Hz
Batteries	
bus = [5 9 10]	
$\bar{P}_g$ = [-0.2 0.3 0.15] pu	$\bar{Q}_g$ = [0 0 0] pu
$R_f = 0.1\ \Omega$	$L_f = 1.610^{-5}$ H
k_p = diag(8.4, 5.6, 11.2)$10^{-4}\frac{\text{pu}}{\text{pu}}$	
k_q = diag(12.5, 12.5, 12.5)$10^{-4}\frac{\text{pu}}{\text{pu}}$	
Loads	
bus = [3 4 6 7 8 11]	
P_l [0.05 0.0432 0.055 0.0077 0.0588 0.0331] pu	
Q_l [0 0 0.0105 0 0 0] pu	

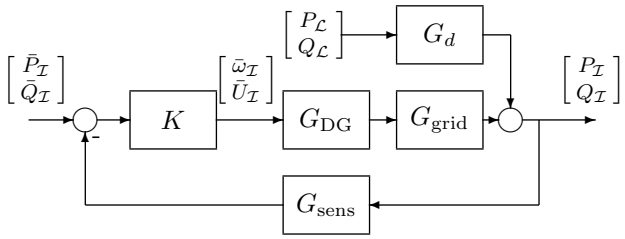

Fig. 2. Block diagram of the full grid model.

Then, using the transfer functions derived above, the complete dynamic phasor model is formed. The impedances of the VSI output filters are lumped with the lines. The block diagram of the model is shown in Fig. 2. The block $K = \text{diag}(kp, kq)$ denotes the transfer function matrix of the droop controller. The sensor dynamics G_{sens} of the power measurements are modeled by a first-order lowpass filter with a cut-off frequency of 5 Hz.

Both the Simpower model and the dynamic phasor model are then simulated, and the response to a step increase of the load at bus 3 at t=1 s by 712.5 kW is compared. For reasons of space, only the active and reactive output power of the VSI at bus 10 are plotted in Fig. 3. The results show that the dynamic phasor model represents well the transient dynamics occurring after a load step, and is well suited for small-signal stability analysis and control design. As the dynamic phasor model is a linear approximation of the power flow equations, an steady-state error can be observed after the disturbance. However, the error is small compared to the size of the disturbance.

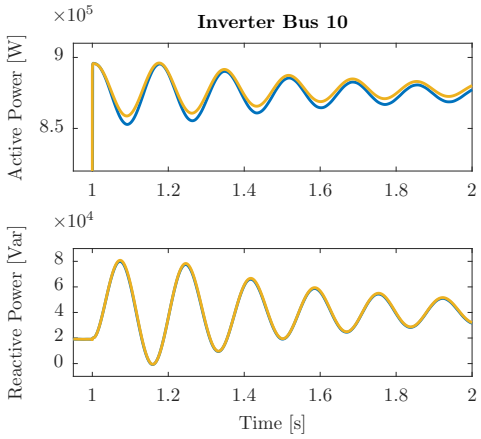

Fig. 3. Active and reactive power of the inverter at bus 10 after an active power load step. Blue is the Simpower simulation, yellow is the dynamic phasor model.

3. IMPROVING TRANSIENT PERFORMANCE

Grid transient stability and performance is a major issue when connecting multiple VSIs in parallel configuration. The typically short lines in distribution grids result in a strong coupling between the inverters, which introduces undesired dynamics. As can be seen in Fig 3, even for the idealized inverter model used in this example the response is underdamped, leading to a bad transient performance with excessive ringing.

Therefore, in this section a novel approach to fixed-structure, robust control design based on the frequency response of multivariable systems and convex optimization is presented. Using the dynamic phasor model developed in the previous section, this method is then used to improve the transient performance of droop control while maintaining proportional load sharing and a decentralized structure. For reasons of space, the method is presented in abbreviated form in this paper. A complete theoretical review can be found in Karimi and Kammer (2016).

3.1 Frequency response data

The system to be controlled is a Linear Time-Invariant multivariable (LTI-MIMO) strictly proper system represented by its frequency response $G(j\omega) \in \mathbf{C}^{n\times n}$, where n is the number of outputs. We assume that $G(j\omega)$ is bounded in all frequencies except for a set B_g including a finite

number of frequencies that correspond to the poles of G on the imaginary axis. We consider $\omega \in \Omega = \mathbf{R} \backslash B_g$.

3.2 Controller Structure

As the design takes place purely in the frequency domain, it is possible to directly design a discrete-time controller while using the frequency response of the continuous-time plant. A fixed-structure discrete-time matrix transfer function controller is considered and defined as:

$$K(z) = X(z)Y^{-1}(z) \tag{8}$$

where $X(z)$ and $Y(z)$ are polynomial matrices in z for discrete-time controller design. For a decentralized controller, we have:

$$X(z) = X_p z^p + \cdots + X_1 z + X_0 \tag{9}$$
$$Y(z) = I z^p + \cdots + Y_1 z + Y_0 \tag{10}$$

where $X_i, Y_i \in \mathbf{R}^{n \times n}$ are diagonal matrices containing the controller parameters. Note that $Y(e^{j\omega})$ must be invertible $\forall \omega \in \Omega$.

3.3 Control performance

The control performance is defined as constraints on the norm of weighted sensitivity functions. A very typical performance specification for reference tracking or disturbance rejection is to minimize the following norm:

$$\min_{X,Y} \|W_1 S\|_\infty \tag{11}$$

where $S = (I + GK)^{-1}$ is the sensitivity function and W_1 is the performance weight. In order to limit the control input, the following constraint can be considered:

$$\|W_2 K S\|_\infty < 1 \tag{12}$$

where W_2 is the control input weight. For a stable system $H(z)$, the infinity-norm is defined as:

$$\|H\|_\infty = \sup_\omega \bar{\sigma}[H(e^{j\omega})] \tag{13}$$

Note that the weighting filters can be either in continuous- or discrete-time. Also, note that the boundedness of the spectral norm of H does not guarantee the stability of H.

3.4 Convex Approximation

The performance specifications described in the previous section can be achieved through convex optimization using only the frequency response data of the plant. The performance constraints can be represented by a set of convex-concave constraints, and can then be approximated by an inner convex approximation based on the linearization of the concave parts.

The optimization problem in (11) can be written as:

$$\begin{aligned} &\min_{X,Y} \gamma \\ &\text{subject to:} \\ &(W_1 S)^* (W_1 S) < \gamma I, \qquad \forall \omega \in \Omega \end{aligned} \tag{14}$$

where $(\cdot)^*$ denotes the complex conjugate transpose. Replacing K with XY^{-1} in the constraint gives:

$$[W_1 Y (Y + GX)^{-1}]^* [W_1 Y (Y + GX)^{-1}] < \gamma I \tag{15}$$

Note that the dependency in ω has been omitted for $G(j\omega), K(e^{j\omega})$ and $W_1(e^{j\omega})$ in order to simplify the notation. Multiplying both sides from the right by $(Y + GX)$, and from the left by its complex conjugate, leads to the following matrix inequality:

$$[W_1 Y]^* \gamma^{-1} [W_1 Y] - (Y + GX)^* (Y + GX) < 0 \tag{16}$$

which is a constraint on the difference between two quadratic terms (a convex-concave constraint). In order to convexify the constraint, the second quadratic term is linearized using the following property:

$$P^* P \geq P^* P_c + P_c^* P - P_c^* P_c \tag{17}$$

where $P = Y + GX$ and P_c is any known complex matrix. We can choose $P_c = Y_c + GX_c$, where $K_c = X_c Y_c^{-1}$ is an initial controller. Using the Schur complement, the constraint in (16) can then represented by an LMI:

$$\begin{bmatrix} P^* P_c + P_c^* P - P_c^* P_c & (W_1 Y)^* \\ W_1 Y & \gamma I \end{bmatrix} > 0 \tag{18}$$

This convex constraint is a sufficient condition for the spectral constraint in (14) for any choice of $K_c = X_c Y_c^{-1}$. However, this constraint will not necessarily represent a convex set of stabilizing controllers. In fact, every unstable system with no pole on the stability boundary has a bounded spectral norm. The conditions on the linearization of the constraints such that the closed-loop stability can be guaranteed is given in the following theorem.

Theorem 1. Given a strictly proper plant model G, an initial stabilizing controller $K_c = X_c Y_c^{-1}$ with $\det(Y_c) \neq 0, \forall \omega \in \Omega$, and feasible solutions X and Y to the following LMI,

$$(Y + GX)^* (Y_c + GX_c) + (Y_c + GX_c)^* (Y + GX) > 0 \tag{19}$$

for all $\omega \in \Omega$, then the controller $K = XY^{-1}$ stabilizes the closed-loop system if

(1) $\det(Y) \neq 0, \forall \omega \in \Omega$.
(2) The initial controller K_c and the final controller K share the same poles on the stability boundary.

Proof: The proof is given in Karimi and Kammer (2016).

Remark: A necessary and sufficient condition for $\det(Y) \neq 0$ is $Y^* Y > 0$. This constraint is concave and can be linearized to obtain the following sufficient convex constraint:

$$Y^* Y_c + Y_c^* Y - Y_c^* Y_c > 0 \tag{20}$$

Furthermore, the condition in (19) is automatically fulfilled when considering an H_∞ constraint on any closed-loop sensitivity function.

3.5 Controller Design Formulation

The goal is to improve the transient performance of the droop controller while retaining the proportional load sharing capabilities and the decentralized structure. This is achieved by designing a 4th-order controller of the form given in (8) with a sampling time T_s=1 ms. The controller is designed to have the same characteristics as the original droop controller at low frequencies, and to eliminate the ringing after a disturbance. It should be noted that the formulation of the control design objectives for droop control is not typical. The objective of decentralized load sharing demands that the controller gains are fixed at lower frequencies. Also, the controller must not include decentralized integrators, for in this case any bias in the measurements would render the system unstable.

From the block diagram given in Fig.2, the plant is defined as $G = G_{\text{sens}} G_{\text{grid}} G_{\text{DG}}$. To guarantee proportional load

sharing, the DC-gain of the new controller (at $z = 1$) has to be equal to the droop gains. This can be achieved by adding the constraint $X(1)Y(1)^{-1} = \text{diag}(k_p, k_q)$, which can be expressed as:

$$\sum_{i=1}^{p} X_i = \text{diag}(k_p, k_q) \left(\sum_{i=1}^{p-1} Y_i + I \right) \tag{21}$$

As objective function, we choose to minimize $\|W_1 S\|_\infty$, where the weighting filter is chosen as:

$$W_1 = \text{diag}(1, 1, 1, 58.2, 58.2, 58.2)^{-1} \tag{22}$$

The values of the weighting filter serve to normalize the sensitivity of the active and reactive VSI power respectively, and are chosen as follows. Let σ_P, σ_Q be the singular values of the sensitivity of the active and reactive power respectively. The entries of the weighting filter are equal to the inverse of the DC-gain of $\max(\sigma_P)$ and $\max(\sigma_Q)$, respectively. Since the DC-gain of the new controller is constrained to be equal to the droop gains, this normalization remains valid.

Additionally, the weighted input sensitivity $\|W_2 KS\|_\infty$ is constrained in order to reduce the overshoot in the grid frequency and voltage, and to prevent fast input changes to the inverter. This is achieved by choosing W_2 as follows:

$$W_2 = \left(0.09\, \text{diag}(10^{-2}, 10^{-2}, 10^{-2}, 1, 1, 1) B\right)^{-1} \tag{23}$$

The values serve to normalize the input sensitivity accordingly, and are chosen in the same fashion as for W_1. B is a second-order discrete-time Butterworth low-pass filter with a cutoff frequency of 1000 rad/s.

Finally, the stability condition presented in Theorem 1 requires a stabilizing initial controller K_c with the same poles on the stability boundary (the unit circle) as the desired final controller. Since the desired controller does not contain any poles on the stability boundary, an obvious choice is to use the existing droop controller as initial controller. This leads to the following initial values:

$$X_c(z) = \text{diag}(kp, kq) \quad ; \quad Y_c(z) = I \tag{24}$$

3.6 Frequency gridding

The optimization problem formulated in the previous section contains an infinite number of constraints (i.e. $\forall \omega \in \Omega$) and is called a semi-infinite problem. A common approach to handle this type of constraints is to choose a reasonably large set of frequency samples $\Omega_N = \{\omega_1, \ldots, \omega_N\}$ with $\omega_1 \geq 0, \omega_N = \pi / T_s$ and replace the constraints with a finite set of constraints at each of the given frequencies. For this example, the optimization problem is sampled using $N = 300$ logarithmically spaced frequency points in the interval $\Omega_N = \left[10^{-1}, 500\right]$ Hz. Using the linearization presented in Section 3.4, the constraint sets are formulated for each of the N frequency points. This results in the following sampled, convex optimization problem :

$$\min_{X,Y} \gamma$$

subject to:

$$\begin{bmatrix} P^* P_c + P_c^* P - P_c^* P_c & (W_1 Y)^* \\ W_1 Y & \gamma I \end{bmatrix} (j\omega_n) > 0$$

$$\begin{bmatrix} P^* P_c + P_c^* P - P_c^* P_c & (W_2 X)^* \\ W_2 X & I \end{bmatrix} (j\omega_n) > 0$$

$$\left[Y_c^* Y + Y^* Y_c - Y_c^* Y_c \right] (j\omega_n) > 0$$

$$\sum_{i=1}^{p} X_i = \text{diag}(k_p, k_q) \left(\sum_{i=1}^{p-1} Y_i + I \right)$$

for $n = 1, \ldots, N$, where the argument $(j\omega_n)$ denotes a constraint evaluated at frequency ω_n, with $P = Y + GX$ and $P_c = Y_c + GX_c$.

3.7 Iterative algorithm

Any LMI solver can be used to solve this optimization problem and calculate a suboptimal controller K around the initial controller K_c. As we are only solving an inner convex approximation of the original optimization problem, K depends heavily on the initial controller K_c and the performance criterion can be quite far from the optimal value. The solution is to use an iterative approach that solves the optimization problem multiple times, using the final controller K of the previous step as the new initial controller K_c. This choice always guarantees closed-loop stability (assuming the initial choice of K_c is stabilizing). The iterative process can be stopped once the change in the performance criterion is sufficiently small.

3.8 Simulation Results

The optimization problem is formulated in Matlab using Yalmip (see Löfberg (2004)), and solved with Mosek (see MOSEK ApS (2015)). The iteration converges to a final controller in 5 steps, which takes around 5 minutes on a standard desktop computer in our simple implementation.

The model detailed in Section 2.3 is then simulated in Simulink using the Simpower toolbox both for the droop controller and the new controller. At t=1 s the active power of the load at bus 3 is increased by 712.5 kW, and the active and reactive power of each inverter is shown in Figs. 4 and 5. It can be seen that the new controller is able to significantly improve the transient response and eliminate the ringing. It is interesting to note that due to the coupling effects of the mixed lines, for the droop controller the active power load change induces large oscillations in the reactive power of the inverters. The new controller is able to significantly reduce this coupling effect, further reinforcing its superior transient performance. Finally, Fig. 4 also shows that proportional active power sharing is maintained, with the new controller reaching the same steady-state power as the droop controller.

4. CONCLUSION

A new transfer function model based on dynamic phasors for low- and medium-voltage distribution grids was developed. It was shown that the model represents well the electromagnetic and electromechanic dynamics in a meshed grid with mixed lines. Further, a novel method to design fixed-structure robust controllers based on the frequency response of multivariable systems and convex optimization was presented. It was then shown that the method can be used to design decentralized low-order controllers for power grids that satisfy desired performance specifications and guarantee closed-loop stability. Finally, a simulation example of a real medium-voltage distribution grid demonstrated that the new controller achieves a

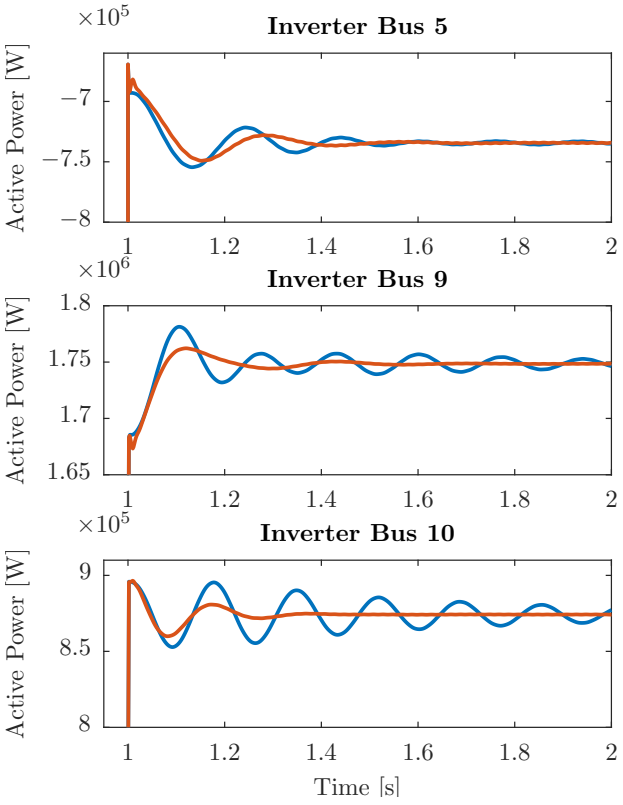

Fig. 4. Active power of each inverter after an active power load step. Blue is the droop controller, red is the new controller.

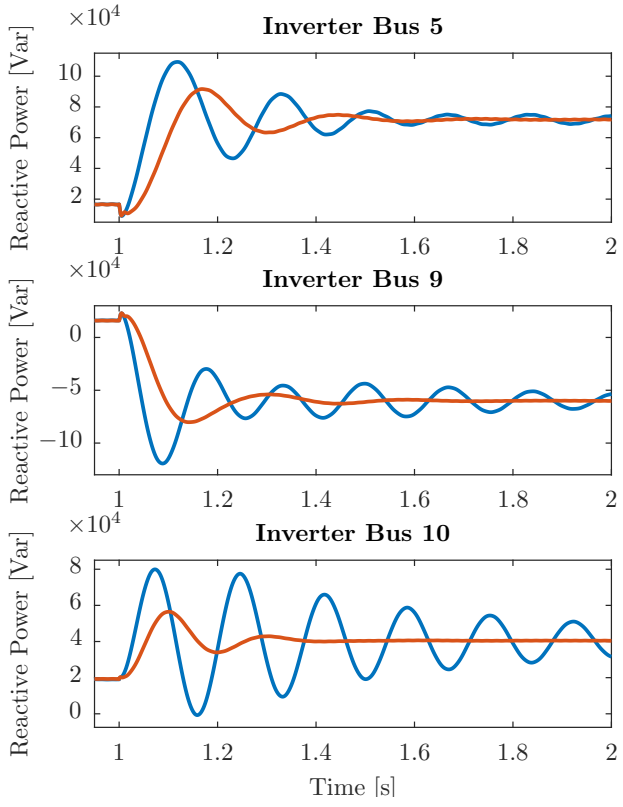

Fig. 5. Reactive power of each inverter after an active power load step. Blue is the droop controller, red is the new controller.

significantly improved transient performance compared to droop control, while maintaining a decentralized structure and guaranteeing proportional load sharing.

REFERENCES

Bidram, A. and Davoudi, A. (2012). Hierarchical structure of microgrids control system. *IEEE Transactions on Smart Grid*, 3(4), 1963–1976.

Brabandere, K.D. (2006). *Voltage and Frequency Droop Control in Low Voltage Grids By Distributed Generators with Inverter Frond-End*. Ph.D. thesis, Katholieke Universiteit Leuven, FACULTEIT INGENIEURSWETENSCHAPPEN, 3001 Leuven, Belgium.

Guerrero, J.M., Matas, J., de Vicuna, L.G., Castilla, M., and Miret, J. (2007). Decentralized control for parallel operation of distributed generation inverters using resistive output impedance. *IEEE Transactions on industrial electronics*, 54(2), 994–1004.

Guerrero, J.M., Vasquez, J.C., Matas, J., de Vicuna, L.G., and Castilla, M. (2011). Hierarchical control of droop-controlled AC and DC microgridsA general approach toward standardization. *IEEE Transactions on Industrial Electronics*, 58(1), 158–172.

Guo, X., Lu, Z., Wang, B., Sun, X., Wang, L., and Guerrero, J.M. (2014). Dynamic phasors-based modeling and stability analysis of droop-controlled inverters for microgrid applications. *IEEE Transactions on Smart Grid*, 5(6), 2980–2987.

Kammer, C. and Karimi, A. (2017). Decentralized and distributed transient control for microgrids. Technical report, EPFL.

Karimi, A. and Kammer, C. (2016). A data-driven approach to robust control of multivariable systems by convex optimization. *arXiv:1610.08776 [math.OC]*.

Löfberg, J. (2004). YALMIP: A toolbox for modeling and optimization in MATLAB. In *CACSD Conference*. `http://control.ee.ethz.ch/joloef/yalmip.php`.

MOSEK ApS (2015). *The MOSEK optimization toolbox for MATLAB manual. Version 7.1.* URL `http://docs.mosek.com/7.1/toolbox/index.html`.

Nazari, M.H. and Ilic, M. (2014). Dynamic modelling and control of distribution energy systems: comparison with transmission power systems. *IET Generation, Transmission & Distribution*, 8(1), 26–34.

Rudion, K., Orths, A., Styczynski, Z., and Strunz, K. (2006). Design of benchmark of medium voltage distribution network for investigation of DG integration. *2006 IEEE Power Engineering Society General Meeting*, 6. doi:10.1109/PES.2006.1709447.

Schiffer, J., Ortega, R., Astolfi, A., Raisch, J., and Sezi, T. (2014). Conditions for stability of droop-controlled inverter-based microgrids. *Automatica*, 50(10), 2457–2469. doi:10.1016/j.automatica.2014.08.009.

Simpson-Porco, J.W., Dörfler, F., and Bullo, F. (2013). Synchronization and power sharing for droop-controlled inverters in islanded microgrids. *Automatica*, 49(9), 2603–2611.

Venkatasubramanian, V., Schattler, H., and Zaborszky, J. (1995). Fast time-varying phasor analysis in the balanced three-phase large electric power system. *IEEE Transactions on Automatic Control*, 40(11), 1975–1982.

Zhong, Q.C. (2013). Harmonic droop controller to reduce the voltage harmonics of inverters.